**Journal of Nuclear Medicine, published on July 17, 2020 as doi:10.2967/jnumed.120.242347**

# Molecular Imaging of Very Late Antigen-4 (VLA-4) in Acute Lung Injury

Joseph Haddad[1], Joseph D. Latoche[2], Shubhanchi Nigam[1], Michael C. Bellavia[3], Kathryn E. Day[2], Qin Zhu[1], W. Barry Edwards[1], Carolyn J. Anderson[1,2,3,4,5], Sina Tavakoli[1,2,5]

Departments of [1]Radiology, [2]Medicine, [3]Bioengineering, and [4]Pharmacology & Chemical Biology, University of Pittsburgh; and [5]Heart, Lung, Blood, and Vascular Medicine Institute, UPMC, Pittsburgh, Pennsylvania

Corresponding Author: Sina Tavakoli, UPMC Presbyterian Hospital, 200 Lothrop Street, Suite E200, Pittsburgh, PA 15213
Phone: 412-647-7288
Fax: 412-647-2601
Email: sit23@pitt.edu

First Author: Joseph Haddad (Postdoctoral Fellow), 3501 Fifth Avenue, Room-10029, Pittsburgh, PA 15213
Phone: 412-294-2777
Fax: 412-647-2601
Email: Joh111@pitt.edu

Sources of Funding: This work was supported by NIH-NHLBI K08-HL144911 and Seed Fund from University of Pittsburgh to S.T; NIH-NCI Cancer Center Support Grant P30-CA047904 (In Vivo Imaging Facility) and NIH-NIAID R01-AI118195.

Running Title: VLA-4 IMAGING IN ACUTE LUNG INJURY

Word Count: 5,000

## ABSTRACT

Inflammation plays a central role in the pathogenesis of acute lung injury (ALI) during both the acute pneumonitis stage and the progression into the chronic fibroproliferative phase, leading to pulmonary fibrosis. Currently, there is an unmet clinical and research need for non-invasive approaches to monitor lung inflammation through targeting immunoregulatory pathways contributing to ALI pathogenesis. In this study, we evaluated the role of targeted imaging of very late antigen-4 (VLA-4), as a key integrin mediating the adhesion and recruitment of immune cells to inflamed tissues, in quantifying lung inflammation in a mouse model of lipopolysaccharide-induced ALI.

**Methods:** ALI was induced by a single intratracheal administration of lipopolysaccharide (10, 20 or 40 μg per mouse) in C57BL/6J mice. Control mice were intratracheally instilled with sterile phosphate-buffered saline. VLA-4-targeted PET/CT was performed 24 hours after intravenous injection of a copper-64 ($^{64}$Cu) labeled high-affinity peptidomimetic ligand, $^{64}$Cu-CB-TE1A1P-PEG$_4$-LLP2A ($^{64}$Cu-LLP2A), at day 2 after the induction of ALI. *Ex vivo* biodistribution of $^{64}$Cu-LLP2A was determined by γ-counting of harvested organs. The severity of lung inflammation was assessed histologically and by measuring the expression of inflammatory markers in the lung tissue lysates using reverse transcription quantitative polymerase chain reaction.

**Results:** Intratracheal lipopolysaccharide instillation led to an acute inflammatory response in the lungs, characterized by increased expression of multiple inflammatory markers and infiltration of myeloid cells, along with a significant and specific increase in $^{64}$Cu-LLP2A uptake, predominantly in a peribronchial distribution. There was a strong correlation between the lipopolysaccharide dose and $^{64}$Cu-LLP2A uptake, as quantified by *in vivo* PET ($R=0.69$, $P<0.01$). Expression levels of both subunits of VLA-4, i.e., integrins $\alpha_4$ and $\beta_1$, significantly correlated with the expression of multiple inflammatory markers, including tumor necrosis factor-α, interleukin-1β and nitric oxide synthase-2, highlighting the potential of VLA-4 as a surrogate marker of acute lung inflammation. Notably, *in vivo* $^{64}$Cu-LLP2A uptake significantly correlated with the expression of multiple inflammatory markers and VLA-4.

**Conclusion:** Our study demonstrates the feasibility of molecular imaging of VLA-4, as a mechanistically-relevant target in ALI, and the accuracy of VLA-4-targeted PET in quantification of ongoing lung inflammation in a murine model.

**Key Words:** acute lung injury, very late antigen-4, molecular imaging, inflammation, PET

## INTRODUCTION

Acute lung injury (ALI) is a clinical syndrome of acute hypoxemic respiratory failure associated with diffuse alveolar damage and bilateral radiographic opacities, not attributable to fluid overload or cardiogenic pulmonary edema (*1*). With an age-adjusted incidence of ~86 per 100,000 person-years and in-hospital mortality rate of ~38% (*1*), ALI is a major health issue, accounting for ~74,500 deaths and 3.6 million hospital days in the USA annually (*1*).

ALI is a heterogeneous syndrome, which may arise from direct exposure to various biological, chemical or physical hazards (e.g., pneumonia, aspiration and toxic fumes) or through indirect insults to the lungs (e.g., sepsis), leading to the disruption of the alveolar-capillary integrity (*2*). Despite this etiologic heterogeneity, an uncontrolled acute inflammatory response, characterized by excessive accumulation of neutrophils, monocytes, and macrophages, and release of pro-inflammatory mediators, is a key pathogenic mechanism shared by different etiologies and a major predictor of mortality in ALI (*3,4*). Additionally, a non-resolving inflammatory response, characterized by continued accumulation of macrophages and fibrocytes/fibroblasts, triggers a fibroproliferative response and is associated with poor prognosis, e.g., prolonged ventilator dependence and high mortality (*5*). This ultimately leads to pulmonary fibrosis, an irreversible sequela of ALI in survivors of the acute pneumonitis phase (*6,7*).

Molecular imaging is an attractive approach to non-invasively track inflammatory processes contributing to ALI pathogenesis (*8,9*), through which prognostication and assessment of disease progression or response to therapy may be improved without the need for invasive diagnostic studies, such as bronchoalveolar lavage and lung biopsy. Among the various molecular imaging approaches, detection of the enhanced metabolic activity of activated immune cells, by $^{18}$F-fluorodeoxyglucose ($^{18}$F-FDG) positron emission tomography (PET) has been extensively exploited in inflammatory diseases, including ALI (*10,11*). However, the limited specificity of $^{18}$F-FDG, which targets a nearly ubiquitous metabolic process, has been a challenge to unravel its biological and clinical implications in inflammatory diseases (*12-14*). This has triggered recent efforts in imaging specific aspects of immune response in ALI, such as infiltration of neutrophils, monocytes and macrophages by targeting chemokine receptor-2 (*8*), folate receptor-β (*9*) and CD11b (*15*), with promising results in preclinical studies.

Very late antigen-4 (VLA-4) is a heterodimeric adhesion molecule, composed of integrins $\alpha_4$ (CD49d) and $\beta_1$ (CD29). Interaction of VLA-4 with its ligands, vascular cell adhesion molecule-1 and fibronectin, plays crucial roles in cell-cell and cell-matrix adhesions required for leukocytes influx in various inflammatory diseases, including pneumonia (*16-18*) and asthma (*19,20*). VLA-4

contributes to the recruitment of neutrophils, monocytes and macrophages in ALI, and its blocking reduces lung inflammation in murine models (*21,22*). Additionally, strong expression of VLA-4 by immune cells infiltrated into the interstitial and alveolar space has been shown in patients with sepsis-induced ALI (*23*). Consistently, VLA-4 is crucial for recruitment of neutrophils and lymphocytes to lungs in *Streptococcus pneumoniae* (*16*) and *Mycobacterium tuberculosis* (*17,18*) pneumonia. These findings strongly support the potential of VLA-4 as a mechanistically-relevant and pharmacologically-intervenable target for molecular imaging of lung inflammation in ALI.

LLP2A is a peptidomimetic ligand with a high affinity to the activated state of VLA-4 with an excellent safety profile and has been used as the targeting moiety of several preclinical theranostic agents in various oncological diseases, such as melanoma (*24-26*) and multiple myeloma (*27,28*), as well as in imaging immune cells in tuberculosis granulomas in a macaque model (*29*). Imaging activated VLA-4 in inflammatory diseases has remained largely unexplored. In this study, we used a previously described LLP2A-derived $^{64}$Cu-labeled tracer, referred to "$^{64}$Cu-LLP2A", which is conjugated with the chelator (1,4,8,11-tetraazacyclotetradecane-1-(methane phosphonic acid)-8-(methane carboxylic acid) (CB-TE1A1P) and a $PEG_4$ linker (*26*), to determine if VLA-4-targeted imaging can quantitatively track the severity of lung inflammation in a murine model of lipopolysaccharide-induced ALI.

## MATERIALS AND METHODS

### Mouse Model of ALI

Adult C57BL/6J mice (N=29) were administered intratracheally with lipopolysaccharide (*Escherichia coli,* O111:B4) or phosphate-buffered saline (PBS). Studies were performed in accordance with a protocol approved by the University of Pittsburgh Institutional Animal Care and Use Committee.

### PET/CT and Quantification of $^{64}$Cu-LLP2A Uptake

Tracer synthesis and radiolabeling were previously described (*26*). Twenty-four hours after lipopolysaccharide (10, 20, or 40-µg) or PBS instillation (N=2 males and 2 females in each group), mice were injected intravenously with $^{64}$Cu-LLP2A (6.4±0.2 MBq). Tracer specificity was addressed in separate groups of male mice (40-µg lipopolysaccharide), imaged with (N=3) or without (N=4) co-injection of ~25 nmol non-labeled LLP2A. Static PET (~10-min) and CT (180 projections, 140-msec exposure, 180° rotation, 80-kVp, 500-µA, field-of-view: 78.5x100-mm)

were performed (Inveon, Siemens) 24-hours after $^{64}$Cu-LLP2A injection. $^{64}$Cu-LLP2A uptake was quantified as standardized uptake value (SUV) (IRW software). Due to the heterogeneous pattern of lung inflammation, we used $SUV_{max}$ rather than $SUV_{mean}$ to avoid under-estimation of tracer uptake. To obtain a representation of total burden of inflammation, lungs were divided into serial non-overlapping zones, each composed of five ~0.8-mm slices. This yielded four-to-five ~4-mm zones after exclusion of apices and bases, which could not be analyzed due to uptake in adjacent organs (thymus and liver). Regions of interest were drawn over the right and left lungs in slices with the highest uptake to determine $SUV_{max}$ in each zone. These $SUV_{max}$ were averaged (4-5 values per each lung) to obtain "average $SUV_{max}$".

Biodistribution was performed by γ-counting (Wizard$^2$, PerkinElmer) of harvested organs. Data are reported as percentage of injected dose per gram tissue (%ID/g) (*26*).

**Gene Expression Assays**

Gene expressions were quantified in right lungs of mice which underwent PET/CT after instillation of 10, 20, or 40-µg lipopolysaccharide or PBS (N=2 males and 2 females per group), per standard methods (*13*) using TaqMan® primers (Supplemental Table 1) and QuantStudio™3 real-time PCR system (Applied Biosystems). Transcript levels are normalized to 18S ribosomal RNA (*Rn18s*) (*12*) and presented relative to the levels in PBS control mice.

**Histology**

Immunohistology of lungs was performed on 10-µm cryosections (Leica-CM1860) in 3 male and 3 female mice instilled with 40 µg lipopolysaccharide or PBS, respectively using commercially-available antibodies (Supplemental Table 2). These mice did not undergo imaging, as lung architecture preservation necessitated inflation by fixative, interfering with measurement of lung weights for biodistribution analysis. Slides were photographed by Axiovert-Microscope.

**Statistical Analysis**

Statistical analysis was performed using Prism-8 (GraphPad). Data are presented as mean±SEM. D'Agostino-Pearson normality test revealed a normal distribution of tracer uptake ($SUV_{max}$ and biodistribution), but non-normal distributions of gene expressions (except for *Cd68* and *Itga4*). Accordingly, one-way analysis of variance, followed by Fisher's Exact post hoc test, was used to compare mean values of tracer uptake in >2 groups (i.e., different lipopolysaccharide doses). Non-paired t-test was performed to compare tracer uptake between blocked and non-blocked groups. Pearson's correlation test was used to determine the associations between *in*

*vivo* and *ex vivo* quantifications of tracer uptake as well as their associations with lipopolysaccharide doses. Non-parametric Kruskal-Wallis analysis, followed by Benjamini-Yekutieli test, was used to compare the expression levels of inflammatory markers between the groups. Associations between tracer uptake and markers of inflammation were determined non-parametrically by Spearman's test. $P<0.05$ was considered statistically significant.

## RESULTS

### Uptake of $^{64}$Cu-LLP2A Correlates with the Inciting Dose of Lipopolysaccharide-Induced ALI

PET/CT performed 24 hours after injection of $^{64}$Cu-LLP2A demonstrated heterogeneous tracer accumulation, predominantly localized in a peri-bronchial distribution, in mice which were intratracheally instilled with lipopolysaccharide, but not PBS (Fig. 1A). *In vivo* PET-derived quantification of $^{64}$Cu-LLP2A uptake (Fig. 1B) demonstrated significant increases in the average $SUV_{max}$ in lungs of mice receiving 40 µg lipopolysaccharide ($SUV_{max}$=0.57±0.06; $P<0.01$) and 20 µg lipopolysaccharide ($SUV_{max}$=0.51±0.06, $P<0.05$), as well as a trend towards significance in those receiving 10 µg lipopolysaccharide ($SUV_{max}$=0.48±0.02, $P=0.08$) *vs.* the PBS control group ($SUV_{max}$=0.37±0.02). Notably, there was a strong correlation between the average $SUV_{max}$ and the inciting dose of lipopolysaccharide (R=0.69, $P<0.01$) (Fig. 1B). No significant difference was present in $^{64}$Cu-LLP2A uptake between male and female mice (though our study was not powered for sex-specific analysis).

Consistent with *in vivo* PET-derived quantification, *ex vivo* quantification by γ-counting demonstrated a ~1.5-fold increase in the $^{64}$Cu-LLP2A uptake in lungs instilled with 40 µg lipopolysaccharide *vs.* PBS (3.63±0.46 *vs.* 2.35±0.19 %ID/g, respectively, $P=0.01$) (Fig. 2A). To verify if quantification of *in vivo* imaging accurately reflects the γ-counting measure of tracer uptake, as the gold standard, we determined the correlation between average $SUV_{max}$ and %ID/g tissue. As shown in Fig. 2A, there was a strong correlation between *in vivo* and *ex vivo* quantification of $^{64}$Cu-LLP2A uptake in the lungs (R=0.77, $P<0.001$).

Consistent with a recent report of intratracheal lipopolysaccharide-induced systemic inflammation and enhanced multi-organ uptake of a $^{64}$Cu-labeled anti-CD11b immuno-tracer (*15*), our *ex vivo* biodistribution studies (Fig. 2B) demonstrated a significant increase in $^{64}$Cu-LLP2A uptake in several organs, including liver, spleen and intestines. There was also a significant increase in the blood pool activity in mice, which received higher doses of lipopolysaccharide (20 and 40 µg) *vs.* PBS.

Specificity of $^{64}$Cu-LLP2A uptake was determined by co-administration of ~200-fold molar excess of non-labeled LLP2A to mice instilled with 40 µg lipopolysaccharide. This reduced lung uptake of $^{64}$Cu-LLP2A by ~50%, as determined by $SUV_{max}$ and γ-counting (Supplemental Fig. 1). Interestingly, there were significant decreases in $^{64}$Cu-LLP2A uptake in additional organs (e.g., thymus, spleen, and bone), but not in the blood pool, indicating specific uptake of $^{64}$Cu-LLP2A secondary to lipopolysaccharide-induced systemic inflammation.

**VLA-4 Expression is a Surrogate Marker of Acute Inflammation in Lipopolysaccharide-Induced ALI**

Intense infiltration of immune cells, most notably neutrophils, monocytes and macrophages, is a critical process in the pathogenesis of ALI (*3,4,8,9,21,22*). Consistently, our immunofluorescent staining showed an abundance of cells expressing myeloid markers, CD11b, Ly6G and CD68, in the lungs of mice treated with intratracheal lipopolysaccharide compared to those receiving PBS (Fig. 3). In addition, there was an increase in the abundance of cells expressing $\alpha_4$ integrin subunit of VLA-4 in lipopolysaccharide-treated *vs.* PBS-treated lungs. We further quantified the severity of lung inflammation by assessing the transcription level of a panel of inflammatory markers. As summarized in a heat map (Fig. 4), there was a robust increase in the expression of several markers of acute inflammation, most pronounced in 40-µg lipopolysaccharide *vs.* PBS control group, including *Cd68* (15-fold), *Mpo* (18-fold), *Ly6g* (72-fold), *Nos2* (73-fold), *Tnf* (70-fold), *Il1b* (500-fold), and *Il12* (17-fold).

In order to determine whether VLA-4 expression quantitatively tracks the severity of lung inflammation, thereby serving as a surrogate target for imaging, we assessed the correlations between VLA-4 subunits (i.e. integrin $\alpha_4$ (*Itga4*) and $\beta_1$ integrin (*Itgb1*)) and the above markers of inflammation (Fig. 5A and 5B). *Itga4* mRNA expression was significantly correlated with *Ly6g* (R=0.63, *P*=0.01), *Cd68* (R=0.85, *P*<0.001), *Nos2* (R=0.80, *P*<0.001), *Tnf* (R=0.70, *P*<0.01), *Il1b* (R=0.58, *P*=0.02) and *Il12* (R=0.81, *P*<0.001) levels. There was also a trend towards modest correlations between the expression of *Itga4* and *Mpo* (R=0.43, *P*=0.10). Moreover, *Itgb1* expression was significantly correlated with *Mpo* (R=0.81, *P*<0.001), *Ly6g* (R=0.75, *P*=0.001), *Cd68* (R=0.70, *P*<0.01), *Nos2* (R=0.59, *P*=0.02), *Tnf* (R=0.65, *P*<0.01), and *Il1b* (R=0.82, *P*<0.001).

***In Vivo* Uptake of $^{64}$Cu-LLP2A Parallels the Severity of Acute Inflammation in ALI**

We next determined whether *in vivo* uptake of $^{64}$Cu-LLP2A reflects the extent of ongoing lung inflammation by assessing the correlations between the $SUV_{max}$ and the expression of VLA-

4 and other inflammatory markers in the corresponding right lung (Fig. 6). Significant correlations were noted between $^{64}$Cu-LLP2A uptake and expression of *Mpo* (R=0.68, *P*<0.01), *Cd68* (R=0.53, *P*=0.04), *Nos2* (R=0.63, *P*=0.01), and *Il1b* (R=0.60, *P*=0.01). Correlations between $SUV_{max}$ and other markers also trended towards significance, including *Itga4* (R=0.51, *P*=0.05), *Igtb1* (R=0.46, *P*=0.08), *Tnf* (R=0.49, *P*=0.06), and *Il12* (R=0.44, *P*=0.10), though these were modest in strength.

## DISCUSSION

Our study demonstrates significant correlations between the expression of VLA-4 and multiple inflammatory markers in a mouse model of lipopolysaccharide-induced ALI, highlighting its role as a biomarker of acute lung inflammation. We also show the feasibility, specificity, and accuracy of quantitative *in vivo* VLA-4-targeted PET, using $^{64}$Cu-LLP2A, to track the severity of inflammation in ALI throughout a range of inciting lipopolysaccharide doses.

An acute inflammatory response, manifesting as intense infiltration of lungs by immune cells, predominantly neutrophils and monocytes/macrophages (*3*), and release of pro-inflammatory mediators, is a hallmark of ALI (*3,30*). The release of various proteolytic enzymes, reactive oxygen and nitrogen species, and cytokines by infiltrated leukocytes plays a critical role in ALI pathogenesis through disrupting the alveolar endothelial-epithelial barrier. Additionally, a longstanding non-resolving inflammatory response causes irreversible lung damage that ultimately leads to lung fibrosis (*6*). Consistent with previous reports (*8,9,21,24,26*), immunohistology demonstrates accumulation of myeloid cells in ALI. This was confirmed quantitatively by distinctly higher transcript levels of myeloid markers in lipopolysaccharide-treated lungs *vs.* PBS controls. Moreover, our data indicated a robust increase in the expression of several other markers of acute inflammation in ALI, including *Mpo*, *Tnf*, *Il1b*, *Il12* and *Nos2*.

Increasing preclinical evidence supports the promising role of molecular imaging in non-invasive detection of various aspects of myeloid cell biology in ALI (*8,9,15*). For example, $^{64}$Cu-labeled anti-CD11b (*15*) and $^{64}$Cu-DOTA-ECL1i, a $^{64}$Cu-labeled tracer targeting chemokine receptor-2, (*8*) have been successfully used in imaging of lipopolysaccharide-induced ALI. Expression of folate receptor-β by activated macrophages has also been exploited for optical imaging of lipopolysaccharide-induced lung inflammation (*9*).

Here, we evaluated the role of targeted imaging of VLA-4 as a key adhesion molecule in promoting the migration of immune cells to inflammatory sites to quantify acute lung inflammation. The number of VLA-4-expressing hematopoietic progenitor cells increases and peaks by ~48

hours after intratracheal administration of lipopolysaccharide, coinciding with the raised level of cytokines in bronchoalveolar lavage fluid (*31*). VLA-4-expressing neutrophils and monocytes have also been shown to infiltrate lung interstitium and alveolar space during ALI (*22,23,32*). The mechanistic role of VLA-4 in recruitment of myeloid cells to lungs has been confirmed through pre-treatment with an anti-VLA-4 blocking antibody in a murine model of lipopolysaccharide-induced ALI (*22,32*). Consistently, our results demonstrate significant correlations between the expression levels of $\alpha_4$ and $\beta_1$ integrin subunits of VLA-4 and multiple markers of acute inflammation, supporting the premise to non-invasively target VLA-4 as a mechanistically-relevant imaging biomarker of lung inflammation. Correlations of $\alpha_4$ and $\beta_1$ subunits with a few inflammatory markers were modest, but trended towards significance, presumably due to differential expression of VLA-4 subunits among different subtypes and/or activation states of leukocytes.

Several pharmacokinetic and pharmacodynamic features of LLP2A have made it an excellent theranostic agent, including its high and selective affinity towards activated VLA-4 (in low nanomolar range), promoting receptor-mediated tracer internalization, its resistance to plasma proteases conferred by its unnatural amino acids, compatibility with various derivatization allowing to achieve a high molar activity, optimal bioavailability, and excellent safety profile (*27,33*). While LLP2A-derived theranostic agents have been extensively investigated in oncological studies (*24-28*), their roles in molecular imaging of inflammatory diseases has remained largely unexplored (*29*). Considering the well-established role of VLA-4 in the recruitment of immune cells, specifically its role in leukocytes influx into inflamed lungs (*16-23,34*), we sought to determine if $^{64}$Cu-LLP2A PET allows for quantitative imaging of inflammation in ALI.

In this study, we show focal areas of $^{64}$Cu-LLP2A uptake localize predominantly in a peri-bronchial distribution, corresponding to the expected pattern of inflammation in intratracheal lipopolysaccharide-induced ALI (*35*). Given this spatial heterogeneity in the inflammatory response, we quantified $^{64}$Cu-LLP2A uptake as the average of $SUV_{max}$ in non-overlapping zones of each lung, as an indicator of overall burden of lung inflammation. This quantification approach avoids the underestimation of the inflammatory burden by employing $SUV_{mean}$, which is influenced by inclusion of non-inflamed lung regions. The significant correlations between *in vivo* quantification of $^{64}$Cu-LLP2A and *ex vivo* uptake determined by γ-counting, as well as administered lipopolysaccharide dose support the accuracy of this quantification approach to track the biodistribution and extent of lung inflammation. A notable finding is the presence of significant correlations between *in vivo* quantification of $^{64}$Cu-LLP2A and expression levels of integrins $\alpha_4$ and $\beta_1$ as well as multiple pro-inflammatory markers, supporting the potential role of

$^{64}$Cu-LLP2A in imaging acute inflammation in ALI. The strengths of correlations between $^{64}$Cu-LLP2A uptake and a few inflammatory markers, including *Mpo*, *Nos2* and *Il1b*, were stronger compared to others, particularly *Ly6g* and *Il12*. This finding suggests that VLA-4 expression/activation may be more strongly associated with specific subsets and/or activation states of immune cells in inflamed lungs. Considering the phenotypic diversity of recruited immune cells in ALI and the complex regulation of inflammatory markers beyond their transcription, further investigations are required to address this possibility.

Consistent with the results of a recent study involving systemic inflammation induced by intratracheal lipopolysaccharide detectable by $^{64}$Cu-labeled anti-CD11b PET (*15*), our biodistribution analysis showed higher levels of $^{64}$Cu-LLP2A in multiple organs, including liver, spleen, intestine, kidneys, and heart, as well as blood, indicating a multi-organ inflammatory response to lipopolysaccharide. Similarly, blood pool activity was higher in mice receiving high doses of lipopolysaccharide (20 and 40 μg), presumably secondary to peripheral blood leukocytosis, which occurs as part of the systemic inflammatory response during the acute phase of lipopolysaccharide-induced ALI (*35*), and increased binding of tracer to VLA-4-expressing circulating cells. We also noted a significant decrease in thymic uptake of $^{64}$Cu-LLP2A in response to the low dose (10 μg) of lipopolysaccharide, speculatively representing the mobilization of VLA-4-expressing cells, including lymphocytes.

## CONCLUSION

Consistent with the mechanistical role of VLA-4 in leukocyte recruitment to inflamed lungs (*16-22,34*), our study highlights the role of VLA-4 as a biomarker of acute lung inflammation and the feasibility of quantitative $^{64}$Cu-LLP2A PET in non-invasive tracking of ongoing inflammation in ALI. The excellent safety profile and correlation of $^{64}$Cu-LLP2A uptake in lungs with lipopolysaccharide dose underscores the translational potential of VLA-4-targeted imaging, which may be utilized towards a precision approach for risk stratification and management of ALI.

**DISCLOSURE:** No potential conflicts of interest.

**KEY POINTS**

QUESTION: Can VLA-4-targeted PET non-invasively monitor the severity of lung inflammation in ALI?

PERTINENT FINDINGS: Lung uptake of $^{64}$Cu-LLP2A correlates with the inciting dose of intratracheal lipopolysaccharide and expression of pro-inflammatory markers in a mouse model of ALI.

IMPLICATIONS FOR PATIENT CARE: Quantitative $^{64}$Cu-LLP2A PET is a feasible and translatable approach for non-invasive tracking of lung inflammation, which may be utilized towards a precision approach to ALI.

## REFERENCES


**1.** Rubenfeld GD, Caldwell E, Peabody E, et al. Incidence and outcomes of acute lung injury. *N Engl J Med.* 2005;353:1685-1693.

**2.** Shaver CM, Bastarache JA. Clinical and biological heterogeneity in acute respiratory distress syndrome: direct versus indirect lung injury. *Clin Chest Med.* 2014;35:639-653.

**3.** Proudfoot AG, McAuley DF, Griffiths MJ, Hind M. Human models of acute lung injury. *Dis Model Mech.* 2011;4:145-153.

**4.** Johnson ER, Matthay MA. Acute lung injury: epidemiology, pathogenesis, and treatment. *J Aerosol Med Pulm Drug Deliv.* 2010;23:243-252.

**5.** Burnham EL, Janssen WJ, Riches DW, Moss M, Downey GP. The fibroproliferative response in acute respiratory distress syndrome: mechanisms and clinical significance. *Eur Respir J.* 2014;43:276-285.

**6.** Wu C, Evans CE, Dai Z, et al. Lipopolysaccharide-induced endotoxemia in corn oil-preloaded mice causes an extended course of lung injury and repair and pulmonary fibrosis: A translational mouse model of acute respiratory distress syndrome. *PLoS One.* 2017;12:e0174327.

**7.** Park PK, Cannon JW, Ye W, et al. Incidence, risk factors, and mortality associated with acute respiratory distress syndrome in combat casualty care. *J Trauma Acute Care Surg.* 2016;81:S150-S156.

**8.** Liu Y, Gunsten SP, Sultan DH, et al. PET-based imaging of chemokine receptor 2 in experimental and disease-related lung inflammation. *Radiology.* 2017;283:758-768.

**9.** Han W, Zaynagetdinov R, Yull FE, et al. Molecular imaging of folate receptor beta-positive macrophages during acute lung inflammation. *Am J Respir Cell Mol Biol.* 2015;53:50-59.

**10.** Chen DL, Mintun MA, Schuster DP. Comparison of methods to quantitate 18F-FDG uptake with PET during experimental acute lung injury. *J Nucl Med.* 2004;45:1583-1590.

**11.** Braune A, Hofheinz F, Bluth T, et al. Comparison of static and dynamic (18)F-FDG PET/CT for quantification of pulmonary inflammation in acute lung injury. *J Nucl Med.* 2019;60:1629-1634.

**12.** Tavakoli S, Downs K, Short JD, et al. Characterization of macrophage polarization states using combined measurement of 2-deoxyglucose and glutamine accumulation: Implications for imaging of atherosclerosis. *Arterioscler Thromb Vasc Biol.* 2017;37:1840-1848.

**13.** Tavakoli S, Short JD, Downs K, et al. Differential regulation of macrophage glucose metabolism by macrophage colony-stimulating factor and granulocyte-macrophage colony-stimulating factor: Implications for (18)F FDG PET imaging of vessel wall inflammation. *Radiology.* 2017;283:87-97.

**14.** Tavakoli S, Zamora D, Ullevig S, Asmis R. Bioenergetic profiles diverge during macrophage polarization: implications for the interpretation of 18F-FDG PET imaging of atherosclerosis. *J Nucl Med.* 2013;54:1661-1667.

**15.** Cao Q, Huang Q, Mohan C, Li C. Small-animal PET/CT imaging of local and systemic immune response using (64)Cu-alphaCD11b. *J Nucl Med.* 2019;60:1317-1324.

**16.** Kadioglu A, De Filippo K, Bangert M, et al. The integrins Mac-1 and alpha4beta1 perform crucial roles in neutrophil and T cell recruitment to lungs during Streptococcus pneumoniae infection. *J Immunol.* 2011;186:5907-5915.

**17.** Feng CG, Britton WJ, Palendira U, Groat NL, Briscoe H, Bean AG. Up-regulation of VCAM-1 and differential expansion of beta integrin-expressing T lymphocytes are associated with immunity to pulmonary Mycobacterium tuberculosis infection. *J Immunol.* 2000;164:4853-4860.

**18.** Walrath JR, Silver RF. The alpha4beta1 integrin in localization of Mycobacterium tuberculosis-specific T helper type 1 cells to the human lung. *Am J Respir Cell Mol Biol.* 2011;45:24-30.

**19.** Koo GC, Shah K, Ding GJ, et al. A small molecule very late antigen-4 antagonist can inhibit ovalbumin-induced lung inflammation. *Am J Respir Crit Care Med.* 2003;167:1400-1409.

**20.** Bocchino V, Bertorelli G, D'Ippolito R, et al. The increased number of very late activation antigen-4-positive cells correlates with eosinophils and severity of disease in the induced sputum of asthmatic patients. *J Allergy Clin Immunol.* 2000;105:65-70.

**21.** Mishra A, Guo Y, Zhang L, et al. A Critical role for P2X7 receptor-induced VCAM-1 shedding and neutrophil infiltration during acute lung injury. *J Immunol.* 2016;197:2828-2837.

**22.** Li XC, Miyasaka M, Issekutz TB. Blood monocyte migration to acute lung inflammation involves both CD11/CD18 and very late activation antigen-4-dependent and independent pathways. *J Immunol.* 1998;161:6258-6264.

**23.** Tsokos M, Fehlauer F. Post-mortem markers of sepsis: an immunohistochemical study using VLA-4 (CD49d/CD29) and ICAM-1 (CD54) for the detection of sepsis-induced lung injury. *Int J Legal Med.* 2001;114:291-294.

**24.** Choi J, Beaino W, Fecek RJ, et al. Combined VLA-4-targeted radionuclide therapy and immunotherapy in a mouse model of melanoma. *J Nucl Med.* 2018;59:1843-1849.

**25.** Beaino W, Nedrow JR, Anderson CJ. Evaluation of (68)Ga- and (177)Lu-DOTA-PEG4-LLP2A for VLA-4-Targeted PET Imaging and Treatment of Metastatic Melanoma. *Mol Pharm.* 2015;12:1929-1938.

**26.** Beaino W, Anderson CJ. PET imaging of very late antigen-4 in melanoma: comparison of 68Ga- and 64Cu-labeled NODAGA and CB-TE1A1P-LLP2A conjugates. *J Nucl Med.* 2014;55:1856-1863.

**27.** Soodgupta D, Zhou H, Beaino W, et al. Ex vivo and in vivo evaluation of overexpressed VLA-4 in multiple myeloma using LLP2A imaging agents. *J Nucl Med.* 2016;57:640-645.

**28.** Soodgupta D, Hurchla MA, Jiang M, et al. Very late antigen-4 (alpha(4)beta(1) Integrin) targeted PET imaging of multiple myeloma. *PLoS One.* 2013;8:e55841.

**29.** Mattila JT, Beaino W, Maiello P, et al. Positron emission tomography imaging of macaques with tuberculosis identifies temporal changes in granuloma glucose metabolism and integrin alpha4beta1-expressing immune cells. *J Immunol.* 2017;199:806-815.

**30.** Cross LJ, Matthay MA. Biomarkers in acute lung injury: insights into the pathogenesis of acute lung injury. *Crit Care Clin.* 2011;27:355-377.

**31.** Trotta T, Di Gioia S, Piro D, et al. Effect of acute lung injury on VLA-4 and CXCR4 expression in resident and circulating hematopoietic stem/progenitor cells. *Respiration.* 2013;85:252-264.

**32.** Burns JA, Issekutz TB, Yagita H, Issekutz AC. The alpha 4 beta 1 (very late antigen (VLA)-4, CD49d/CD29) and alpha 5 beta 1 (VLA-5, CD49e/CD29) integrins mediate beta 2 (CD11/CD18) integrin-independent neutrophil recruitment to endotoxin-induced lung inflammation. *J Immunol.* 2001;166:4644-4649.

**33.** Peng L, Liu R, Marik J, Wang X, Takada Y, Lam KS. Combinatorial chemistry identifies high-affinity peptidomimetics against alpha4beta1 integrin for in vivo tumor imaging. *Nat Chem Biol.* 2006;2:381-389.

**34.** Kenyon NJ, Liu R, O'Roark EM, Huang W, Peng L, Lam KS. An alpha4beta1 integrin antagonist decreases airway inflammation in ovalbumin-exposed mice. *Eur J Pharmacol.* 2009;603:138-146.

**35.** de Souza Xavier Costa N, Ribeiro Junior G, Dos Santos Alemany AA, et al. Early and late pulmonary effects of nebulized LPS in mice: An acute lung injury model. *PLoS One.* 2017;12:e0185474.

# Figure Legends

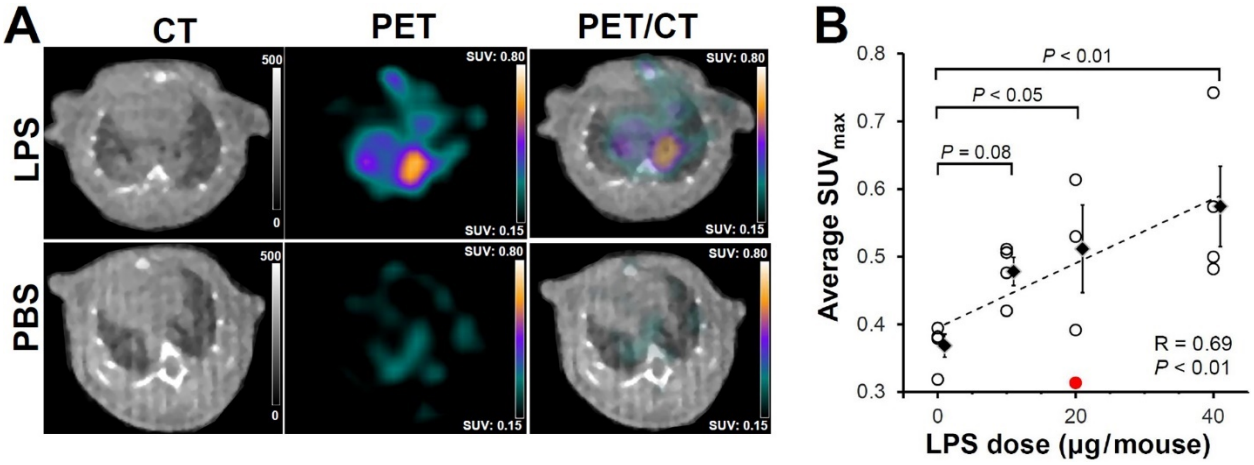


**Figure 1. PET/CT of lung inflammation in lipopolysaccharide-induced ALI.** (A) Representative PET/CT images of mice 2 days after intratracheal administration of 40 µg lipopolysaccharide (top row) or PBS (bottom row) demonstrates heterogeneous uptake of $^{64}$Cu-LLP2A in inflamed lungs with a peri-bronchial distribution. (B) Quantitative analysis demonstrates a significant correlation between $^{64}$Cu-LLP2A uptake and lipopolysaccharide dose. Data points represent the averaged uptake of right and left lungs in each mouse (N=4 per group; red dot in the 20-µg lipopolysaccharide group represents a technical outlier (female), excluded in all subsequent analysis due to the absence of lung inflammation by gene expression assays). LPS=lipopolysaccharide.

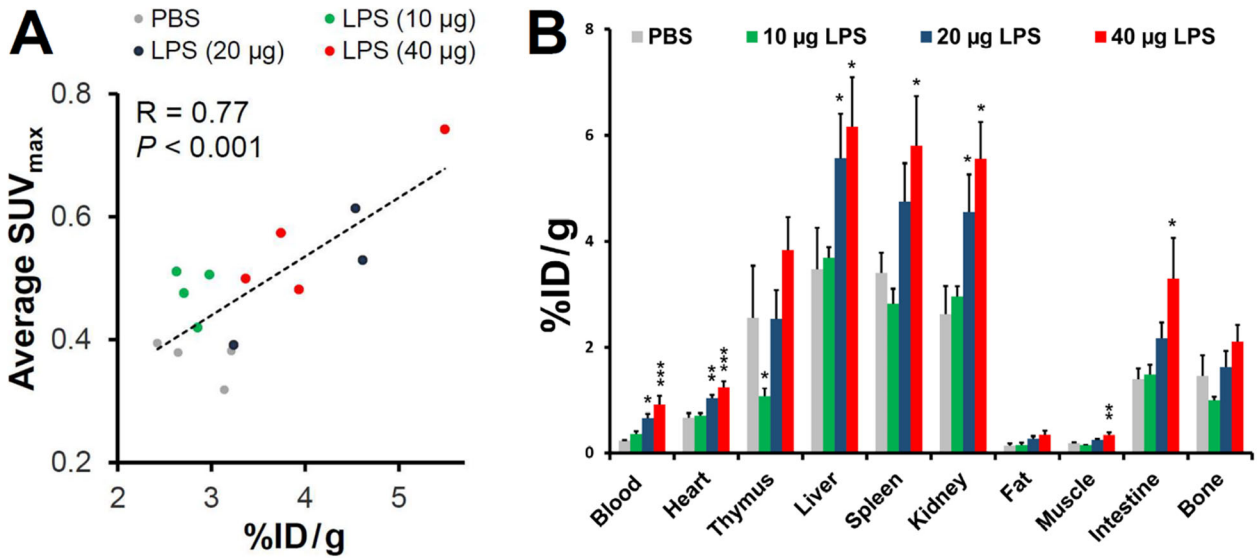


**Figure 2. Biodistribution of $^{64}$Cu-LLP2A.** (A) *In vivo* PET-derived quantification of lung $^{64}$Cu-LLP2A uptake significantly correlates with *ex vivo* quantification of uptake 2 days after induction of ALI. Data points represent the averaged uptake of right and left lungs in each mouse. (B) *Ex vivo* biodistribution of $^{64}$Cu-LLP2A in major organs 24 hours after intravenous administration. Data are expressed as percent injected dose per gram tissue (%ID/g) (N=3 in the 20-μg lipopolysaccharide group and =4 in other groups). **P*<0.05, ***P*<0.01, and ****P*<0.001 compared to PBS control group. LPS=lipopolysaccharide.

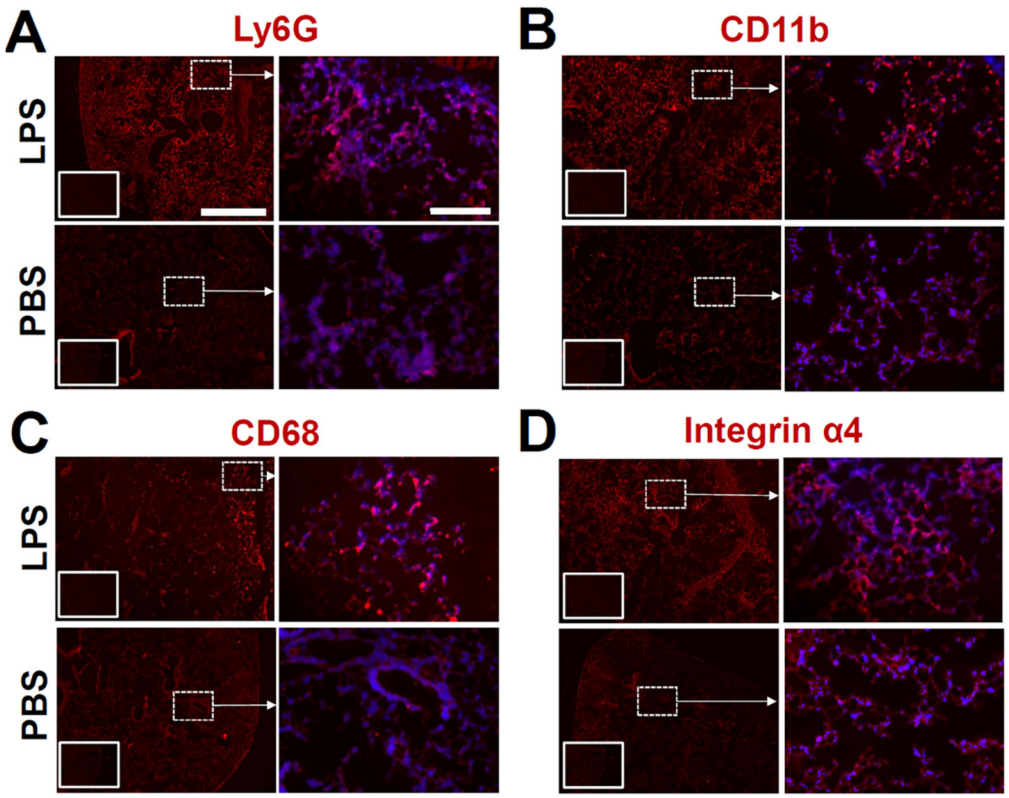


**Figure 3. Immunohistology in lipopolysaccharide-induced ALI**. (A) Representative immunofluorescent staining shows intense infiltration of inflamed lungs after lipopolysaccharide-induced ALI (top rows), compared to PBS controls lungs (bottom rows), by myeloid cells expressing neutrophilic and monocytic/macrophage markers (in red), including Ly6G (A), CD11b (B) and CD68 (C). The abundance of integrin $\alpha_4$-expressing cells is also increased in ALI (D). Right columns in each group represent high-magnification images of the regions demarcated by dashed boxes in low-magnification images in the right columns with overlaid DAPI nuclear staining (blue). The insets in the lower right corner of low-magnification images represent negative control staining. Scale bars indicate 1,000-μm and 200-μm in the low-and high-magnification images, respectively. N=3 per group. LPS=lipopolysaccharide.

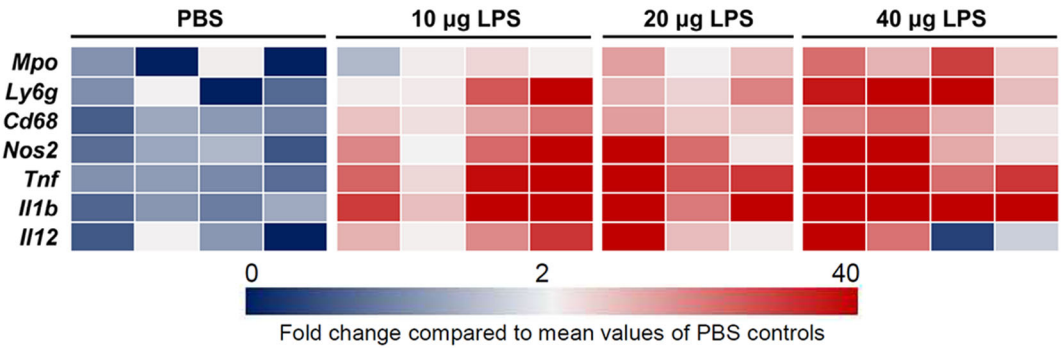


**Figure 4. Induction of lung inflammation by lipopolysaccharide-induced ALI.** Heat map representation confirms a marked increase in mRNA transcripts of several inflammatory markers in inflamed lungs 2 days after the induction of ALI. The expression level of each transcript is demonstrated relative to the average expression in the PBS control group, using a color intensity scale ranging from 0 (dark blue) to >40 (dark red) with the 2-fold values in white. Analyses were performed for the right lung. N=3 in the 20-µg lipopolysaccharide group and =4 in other groups. LPS=lipopolysaccharide.

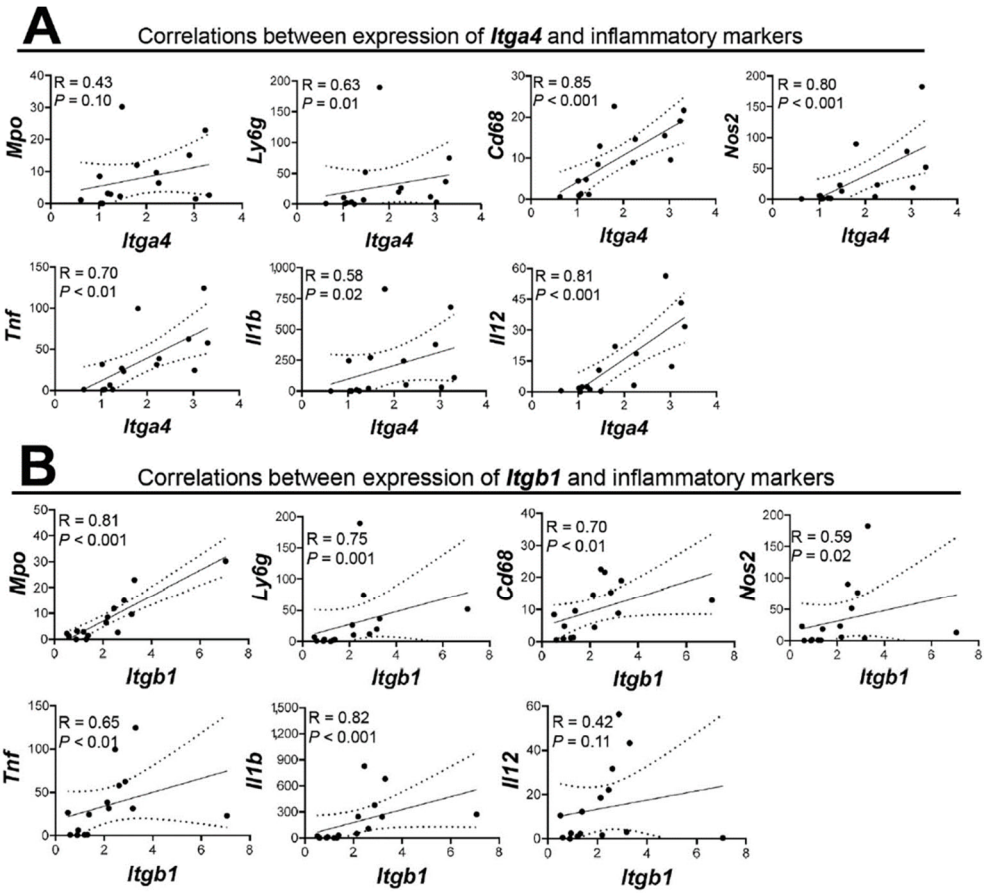


**Figure 5. Correlations between the expression of integrin α4 (*Itga4*) and integrin β1 (*Itgb1*) with markers of lung inflammation.** The expression of both $\alpha_4$ and $\beta_1$ subunits of VLA-4 correlates with the expression levels of various markers of neutrophil and monocyte/macrophage-driven inflammation. Transcript levels are normalized to *Rn18s*. Analyses were performed for the right lung. N=3 in the 20-μg lipopolysaccharide group and =4 in other groups.

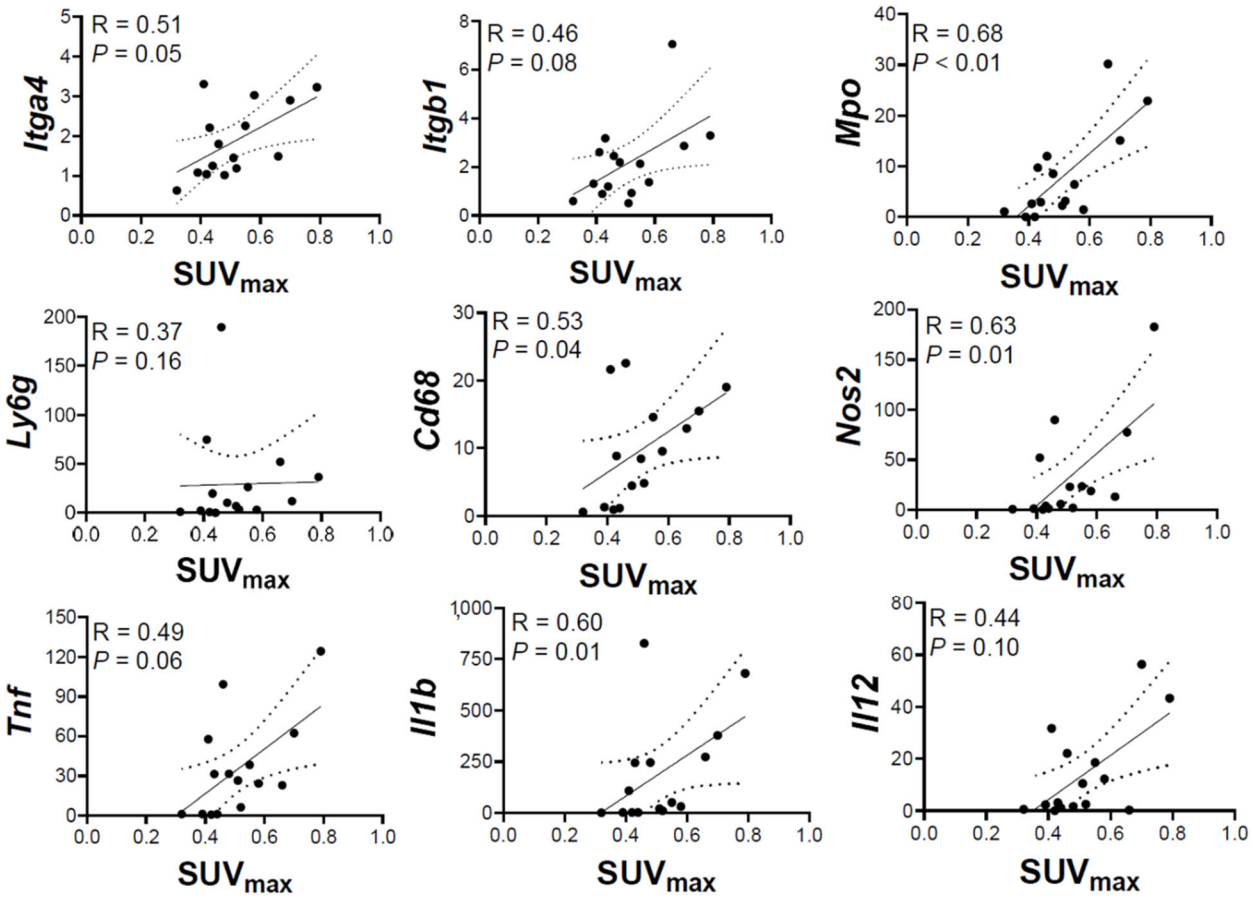


**Figure 6. Correlations between $^{64}$Cu-LLP2A uptake and markers of lung inflammation.** *In vivo* quantification of $^{64}$Cu-LLP2A uptake demonstrates significant correlations between average $SUV_{max}$ and the expression of *Mpo*, *Cd68*, *Nos2*, and *Il1b* in right lungs. There are also trends towards significance between average lung $SUV_{max}$ and expression of *Tnf* (*P*=0.06) and *Il12* (*P*=0.10). Transcript levels are normalized to *Rn18s*. N=3 in the 20-µg lipopolysaccharide group and =4 in other groups.

# Supplemental Data

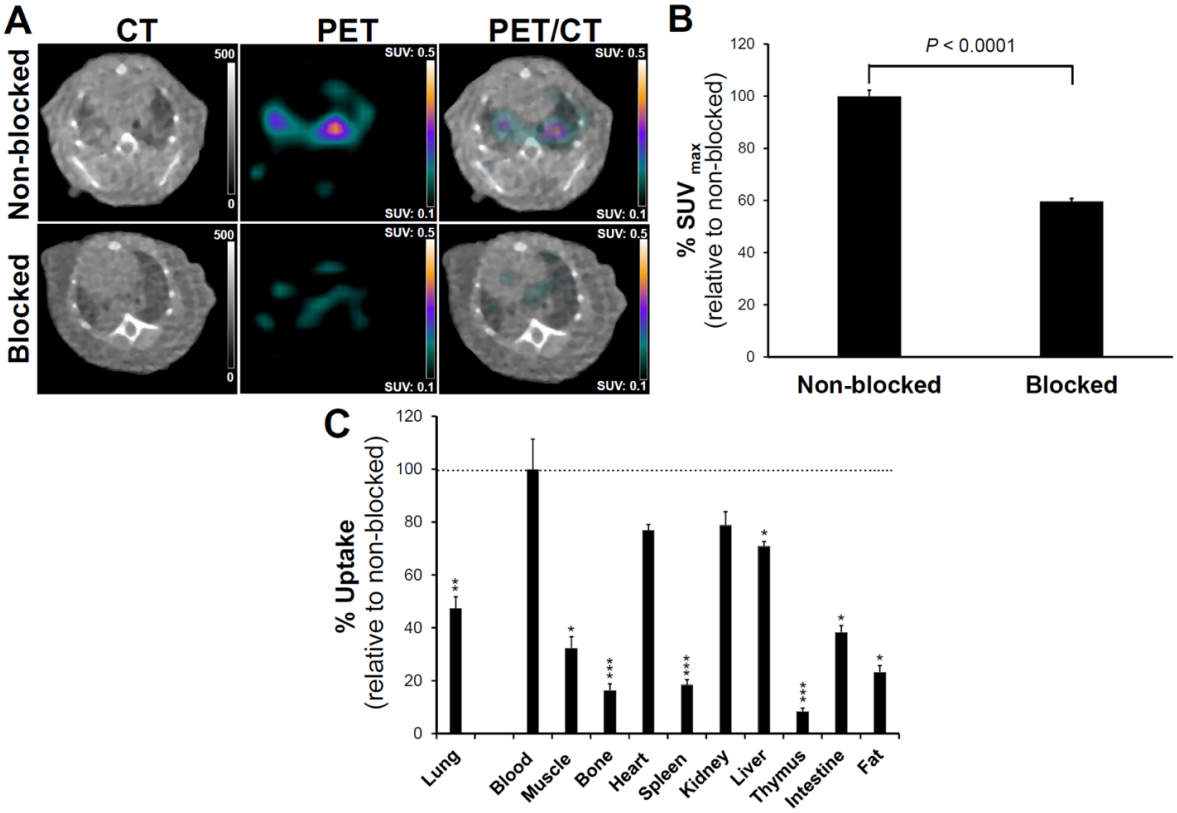


**Supplemental Figure 1. Specificity of $^{64}$Cu-LLP2A uptake.** (A) Representative CT, PET and fused PET/CT images of mice 2 days post intratracheal instillation of 40 µg lipopolysaccharide without (top row: non-blocked) or with (bottom row: blocked) co-administration of non-labeled LLP2A. Visual assessment demonstrates a marked decline in $^{64}$Cu-LLP2A uptake in the inflamed lungs, indicating the specificity of uptake. (B) *In vivo* quantification of PET images confirms a significant reduction in lung uptake of $^{64}$Cu-LLP2A uptake by non-labeled LLP2A (data are expressed as % $SUV_{max}$ in the blocked relative to the non-blocked group). (C) The specificity of $^{64}$Cu-LLP2A uptake is also confirmed by *ex vivo* biodistribution, which demonstrated a significant reduction in $^{64}$Cu-LLP2A in inflamed lungs in the blocked group (data are expressed as the % uptake in the blocked relative to the non-blocked group). Notably, $^{64}$Cu-LLP2A was markedly decreased by co-administration of non-labeled compound in spleen, thymus, and bone where abundant VLA-4 expressing immune or hematopoietic cells reside. N = 4 in the non-blocked group and = 3 in the blocked group. *$P < 0.05$, ** $P < 0.01$, and *** $P < 0.001$ compared to the non-blocked group.

**Supplemental Table 1.** List of TaqMan primers used for quantitative RT-PCR.

| Species | Assay name | Gene full name | Assay ID |
|---|---|---|---|
| Mouse | *Cd68* | CD68 | Mm03047343_m1 |
| | *Il1b* | IL-1β | Mm00434228_m1 |
| | *Il12* | IL-12 | Mm00434174_m1 |
| | *Itga4* | integrin $\alpha_4$ | Mm01277951_m1 |
| | *Itgb1* | integrin $\beta_1$ | Mm01253230_m1 |
| | *Ly6g* | Ly6G | Mm04934123_m1 |
| | *Mpo* | Myeloperoxidase | Mm01298424_m1 |
| | *Nos2* | nitric oxidase synthase-2 | Mm00440502_m1 |
| | *Rn18s* | 18S ribosomal RNA | Mm03928990_g1 |
| | *Tnf* | tumor necrosis factor-α | Mm00443258_m1 |

**Supplemental Table 2.** List of antibodies used for immunostaining.

| Antibody | Clone | Source | Incubation time |
|---|---|---|---|
| anti-mouse CD11b | M1/70 | BioLegend | 60 min |
| anti-mouse CD68 | FA-11 | Bio-Rad Laboratories | 60 min |
| anti-mouse Ly6G | 1A8 | BioLegend | 60 min |
| anti-mouse CD49d | 9C10 | BioLegend | 60 min |
| Cy3-conjugated anti-rat IgG | 712-165-153 | Jackson ImmunoResearch | 45 min |